JACS
JOURNAL OF THE AMERICAN CHEMICAL SOCIETY

ARTICLE

pubs.acs.org/JACS

Helical Water Chain Mediated Proton Conductivity in Homochiral Metal−Organic Frameworks with Unprecedented Zeolitic *unh*-Topology

Subash Chandra Sahoo,* Tanay Kundu, and Rahul Banerjee*

Physical/Materials Chemistry Division, National Chemical Laboratory, Dr. Homi Bhabha Road, Pune 411008, India

Supporting Information

ABSTRACT: Four new homochiral metal−organic framework (MOF) isomers, $[Zn(l\text{-}L_{Cl})(Cl)](H_2O)_2$ (**1**), $[Zn(l\text{-}L_{Br})(Br)](H_2O)_2$ (**2**), $[Zn(d\text{-}L_{Cl})(Cl)](H_2O)_2$ (**3**), and $[Zn(d\text{-}L_{Br})(Br)](H_2O)_2$ (**4**) [L = 3-methyl-2-(pyridin-4-ylmethylamino)-butanoic acid], have been synthesized by using a derivative of L-/D-valine and $Zn(CH_3COO)_2 \cdot 2H_2O$. A three-periodic lattice with a parallel 1D helical channel was formed along the crystallographic *c*-axis. Molecular rearrangement results in an unprecedented zeolitic *unh*-topology in **1**−**4**. In each case, two lattice water molecules (one H-bonded to halogen atoms) form a secondary helical continuous water chain inside the molecular helix. MOFs **1** and **2** shows different water adsorption properties and hence different water affinity. The arrangement of water molecules inside the channel was monitored by variable-temperature single-crystal X-ray diffraction, which indicated that MOF **1** has a higher water holding capacity than MOF **2**. In MOF **1**, water escapes at 80 °C, while in **2** the same happens at a much lower temperature (∼40 °C). All the MOFs reported here shows reversible crystallization by readily reabsorbing moisture. In MOFs **1** and **2**, the frameworks are stable after solvent removal, which is confirmed by a single-crystal to single-crystal transformation. MOFs **1** and **3** show high proton conductivity of 4.45×10^{-5} and 4.42×10^{-5} S cm^{-1}, respectively, while **2** and **4** shows zero proton conductivity. The above result is attributed to the fact that MOF **1** has a higher water holding capacity than MOF **2**.

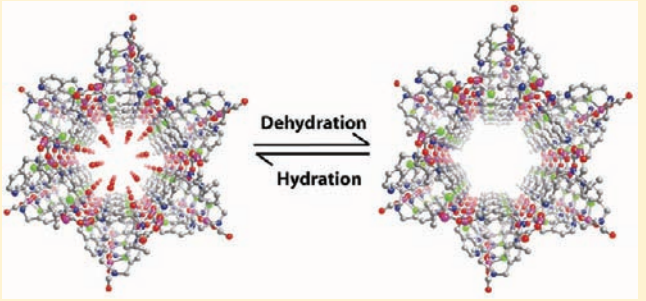

INTRODUCTION

Metal−organic frameworks (MOFs) has gained researchers' attention because of their diverse topological architectures and applications like gas sorption,[1] catalysis,[2] magnetism,[3] and electrical conductivity.[4] Proton (ion) conductivity in solid-state materials is important due to potential applications in transport dynamics, electrochemical devices, and fuel cells, and most importantly to understand the complex biological ion channels.[5] The design and synthesis of new proton conductors are enormously important for clean energy applications, where the efficiency of proton exchange membrane-based fuel cells could be greatly improved in terms of both cost and performance. As a key structural basis, these materials need proton carriers such as H_3O^+ or H^+, given by acid or OH groups, and proton-conducting pathways composed of hydrogen-bond networks for proton conduction. It is well known that nafion has been extensively used as a proton conductor in fuel cells under hydrous conditions. However, nafion suffers a limitation of operating in temperature above 80 °C. Owing to this importance, some deliberate attempts have been made to design inorganic or organic proton conductors[6] such as metal phosphate, oxalate, metal oxides, and organic polymers for applications in fuel cells and sensors.

Application of MOFs in energy-related domains like ion conduction has not been explored as broadly as gas storage and separation, based on available literature reports. The crystallinity of MOFs can provide new breakthroughs in the field of ion conduction, which is often absent in polymer-based electrolytes because of the lack of long-range order. The main advantages of MOFs over other porous materials, like activated carbon and zeolites, is their highly designable nature, which allows not only the size and shape but also the physical properties to be tuned. In particular, the inner surface of MOFs can be tuned with respect to hydrophilicity and acidity via suitable links to control the proton conduction. Still, very limited work on the proton conductivity on MOFs has been reported where either lattice backbone,[7a] added guest molecules like imidazole[7a] and 1,2,4-triazole[4l] in an anhydrous medium, or water chains and clusters[7d] already present inside the framework facilitate proton conduction. Kitagawa et al. have extensively studied proton conductivity in various MOFs where coordinated water or guest molecules play a vital role in proton conduction.[8] However, the role of halogens (especially halogens coordinated to metals) in controlling proton conduction in MOFs has not been explored at all. Here we present a series of four chiral MOFs with an unprecedented zeolitic *unh*-topology which contains a helical continuous

Received: August 19, 2011
Published: September 15, 2011

dx.doi.org/10.1021/ja2078637 | *J. Am. Chem. Soc.* 2011, 133, 17950–17958

water chain inside the pores. MOFs $[Zn(l\text{-}L_{Cl})(Cl)](H_2O)_2$ (**1**) and $[Zn(d\text{-}L_{Cl})(Cl)](H_2O)_2$ (**3**), due to this helical water chain, exhibit a high proton conductivity of $\sim 4.45 \times 10^{-5}$ S cm^{-1} at ambient temperature, while MOFs $[Zn(l\text{-}L_{Br})(Br)](H_2O)_2$ (**2**) and $[Zn(d\text{-}L_{Br})(Br)](H_2O)_2$ (**4**) show almost zero proton conductivity, even though all four MOFs adopt similar architectures [L= 3-methyl-2-(pyridin-4-ylmethylamino)butanoic acid]. It is noteworthy that 1D water chains have become a domain of interest because of their crucial role in the biological transport of protons and ions.[9] We have also provided evidence for proton conduction due to the helical water chain by variable-temperature proton conduction and D_2O exchange experiments. Though many such helical water chains exist in synthetic complexes, there are only a handful of reports where a 1D water chain exists as the default chain after MOF synthesis, because in most cases high-boiling solvents like DMF, DEF, DMA, and DMSO are used instead of water.[10] These MOFs **1**−**4** are characterized by single-crystal X-ray diffraction (SCXRD), thermogravimetric analysis (TGA), powder X-ray diffraction (PXRD), circular dichroism (CD), and hot-stage microscopy. The mobility of the water molecule with respect to temperature has been monitored by in situ variable-temperature powder X-ray diffraction (VT-PXRD) and single-crystal to single-crystal (SC-SC) transformation experiments. The ordered water molecules anchored by weak metal−halogen groups facilitate proton conduction, as confirmed by proton conductivity measurements coupled with deuterium exchange and solid-state (SS) NMR experiments.

EXPERIMENTAL PROCEDURES

Materials and General Methods. All reagents were commercially available and used as received. Powder X-ray diffraction patterns were recorded on a Phillips PANalytical diffractometer with Cu Kα irradiation (λ = 1.5406 Å), a scan speed of 2° min^{-1}, and a step size of 0.02° in 2θ. Fourier transform (FT) IR spectra (KBr pellet) were obtained on a Perkin Elmer FT-IR spectrometer (Nicolet). Thermogravimetric analysis was carried out in the temperature range of 25−800 °C on an SDT Q600 TG-DTA analyzer under a N_2 atmosphere at a heating rate of 10 °C min^{-1}. All low-pressure CO_2 adsorption experiments (up to 1 bar) were performed on a Quantachrome Quadrasorb automatic volumetric instrument. All low-pressure water adsorption experiments (up to 1 bar) were performed on a BELSORP-max volumetric instrument. A Leica M-80 optical microscope with hot stage and camera attachment was used for collecting photographs. Proton conductivity data were measured by a quasi-two-probe method, with a Solartron 1287 electrochemical interface and a frequency response analyzer; circular dichroism data were measured with a JASCO J-851-150L CD spectropolarimeter. Solid-state NMR spectra were recorded with a Bruker 300 MHz NMR spectrometer, and ligand NMR spectra were recorded with a Bruker 200 MHz NMR spectrometer.

Synthesis. *N-(4-Pyridylmethyl)-L-valine·HCl [**l-L$_{Cl}$**].* The ligand *N*-(4-pyridylmethyl)-L-valine·HCl (*l*-L_{Cl}) was prepared using a modified literature procedure.[11] To an aqueous solution (10 mL) of L-valine (2 g, 17 mmol) and Na_2CO_3 (0.91 g, 8.5 mmol), 4-pyridinecarboxaldehyde (1.82 g, 17 mmol) in MeOH (10 mL) was added slowly. The solution was stirred for 1 h and cooled in an ice bath. $NaBH_4$ (0.76 g, 20.4 mmol) in 10 mL of water was added. The mixture was stirred for 1 h, and 3 N HCl was used to adjust the pH to 5−6. The solution was stirred further for 2 h and then evaporated to dryness. The solid was extracted in hot and dry MeOH (150 mL × 3), and the filtrate was evaporated to get a white powder. Yield: 2.9 g, 70% yield. IR (KBr, cm^{-1}): ν_{OH}, 3421; $\nu_{as}(CO_2)$, 1562; $\nu_s(CO_2)$, 1409. ^{1}H NMR (D_2O, ppm): -CH_3 (1.21, d, 3H), -CH_3 (1.35, d, 3H), -CH (3.20, m, 1H), -HN-CH (3.65, m, 1H), -CH_2 (3.82, dd, 2H), py-H (7.34, d, 2H), py-H (8.38, d, 2H).

*N-(4-Pyridylmethyl)-L-valine·HBr [**l-L$_{Br}$**].* The ligand *N*-(4-pyridylmethyl)-L-valine·HBr (*l*-L_{Br}) was prepared exactly as *l*-L_{Cl}, except HBr was used instead of HCl for pH adjustment. Yield: 3.4 g, 70%. IR (KBr, cm^{-1}): ν_{OH}, 3420; $\nu_{as}(CO_2)$, 1560; $\nu_s(CO_2)$, 1411. ^{1}H NMR (D_2O, ppm): -CH_3 (1.20, d, 3H), -CH_3 (1.33, d, 3H), -CH (3.24, m, 1H), -HN-CH (3.63, m, 1H), -CH_2 (3.79, dd, 2H), py-H (7.34, d, 2H), py-H (8.37, d, 2H).

*N-(4-Pyridylmethyl)-D-valine·HCl [**d-L$_{Cl}$**].* The ligand *N*-(4-pyridylmethyl)-D-valine·HCl (*d*-L_{Cl})was prepared exactly as (*l*-L_{Cl}), except D-valine was used instead of L-valine. Yield: 3.1 g, 72%. IR (KBr, cm^{-1}): ν_{OH}, 3417; $\nu_{as}(CO_2)$, 1564; $\nu_s(CO_2)$, 1415. ^{1}H NMR (D_2O, ppm): -CH_3 (1.21, d, 3H), -CH_3 (1.34, d, 3H), -CH (3.22, m, 1H), -HN-CH (3.65, m, 1H), -CH_2 (3.78, dd, 2H), py-H (7.30, d, 2H), py-H (8.36, d, 2H).

*N-(4-Pyridylmethyl)-D-valine·HBr [**d-L$_{Br}$**].* The ligand *N*-(4-pyridylmethyl)-D-valine·HBr (*d*-L_{Br}) was prepared exactly as *l*-L_{Br}, except D-valine was used instead of L-valine. Yield, 3.6 g, 72% . IR (KBr, cm^{-1}): ν_{OH}, 3419; $\nu_{as}(CO_2)$, 1570; $\nu_s(CO_2)$, 1421. ^{1}H NMR (D_2O, ppm): -CH_3 (1.20, d, 3H), -CH_3 (1.34, d, 3H), -CH (3.24, m, 1H), -HN-CH (3.63, m, 1H), -CH_2 (3.80, dd, 2H), py-H (7.35, d, 2H), py-H (8.37, d, 2H).

*$[Zn(l\text{-}L_{Cl})(Cl)](H_2O)_2$ (**1**).* To an aqueous solution (2 mL) of *l*-L_{Cl} (0.044 g, 0.2 mmol), $Zn(CH_3COO)_2 \cdot 2H_2O$ (0.022 g, 0.1 mmol) was added and sonicated for 10 min. The clear solution was kept in a tightly capped 5 mL vial for 24 h at 90 °C to produce rod-shaped transparent crystals. Yield: 0.025 g, 71%. IR (KBr, cm^{-1}): ν_{OH}, 3421; ν_{N-H}, 2977; $\nu_{as}(CO_2)$, 1589; $\nu_s(CO_2)$, 1395; ν_{C-N},1626. Elemental analysis: calcd C (38.8%), H (4.44%), N (8.23%); found C (38.78%), H (4.41%), N (8.25%).

*$[Zn(l\text{-}L_{Br})(Br)](H_2O)_2$ (**2**).* To an aqueous solution (2 mL) of *l*-L_{Br} (0.044 g, 0.2 mmol), $Zn(CH_3COO)_2 \cdot 2H_2O$ (0.022 g, 0.1 mmol) was added and sonicated for 10 min. The clear solution was kept in a tightly capped 5 mL vial for 24 h at 90 °C to produce rod-shaped transparent crystals. Yield: 0.026 g, 67%. IR (KBr, cm^{-1}): ν_{OH}, 3427; ν_{N-H}, 2974; $\nu_{as}(CO_2)$, 1590; $\nu_s(CO_2)$, 1394; ν_{C-N},1623. Elemental analysis: calcd C (34.37%), H (3.90%), N (7.29%); found C (34.35%), H (3.92%), N (7.25%).

*$[Zn(d\text{-}L_{Cl})(Cl)](H_2O)_2$ (**3**).* To an aqueous solution (2 mL) of *d*-L_{Cl} (0.044 g, 0.2 mmol), $Zn(CH_3COO)_2 \cdot 2H_2O$ (0.022 g, 0.1 mmol) was added and sonicated for 10 min. The clear solution was kept in a tightly capped 5 mL vial for 24 h at 90 °C to produce rod-shaped transparent crystals. Yield: 0.023 g, 71%. IR (KBr, cm^{-1}): ν_{OH}, 3420; ν_{N-H}, 2975; $\nu_{as}(CO_2)$, 1589; $\nu_s(CO_2)$, 1397; ν_{C-N}, 1627. Elemental analysis: calcd C (38.82%), H (4.44%), N (8.23%); found C (38.79%), H (4.42%), N (8.24%).

*$[Zn(d\text{-}L_{Br})(Br)](H_2O)_2$ (**4**).* To an aqueous solution (2 mL) of *d*-L_{Br} (0.044 g, 0.2 mmol), $Zn(CH_3COO)_2 \cdot 2H_2O$ (0.022 g, 0.1 mmol) was added and sonicated for 10 min. The clear solution was kept in a tightly capped 5 mL vial for 24 h at 90 °C to produce rod-shaped transparent crystals. Yield: 0.026 g, 69%. IR (KBr, cm^{-1}): ν_{OH}, 3425; ν_{N-H}, 2970; $\nu_{as}(CO_2)$, 1592; $\nu_s(CO_2)$, 1395; ν_{C-N}, 1622. Elemental analysis: calcd C (34.37%), H (3.90%), N (7.29%); found C (34.36%), H (3.91%), N (7.27%).

*$[Zn(l\text{-}L_{Cl})(Cl)]$ (**1′**).* A 1 g sample of MOF **1** was evacuated at 150 °C for 12 h and further characterized by elemental analysis and TGA. A single crystal of **1′** suitable for XRD was obtained by slow thermal heating at a rate of 6 K min^{-1}, and data were collected at various temperature intervals (25−100 °C). It was observed that at 80 °C we could achieve an evacuated framework of **1** with reasonably good data [R_1 = 6.4%, weighted R (wR_2) = 14.7%, goodness-of-fit (GOF) = 1.005]; below that temperature water stays in the lattice as solvent, and above it the framework remains intact but high thermal vibration in the atom

sites results in high refinement parameters. Elemental analysis: calcd C (42.84%), H (4.90%), N (9.0%); found C (42.52%), H (4.74%), N (8.77%).

*[Zn(**d-L$_{Br}$**)(Br)] (**2′**).* A 1 g sample of MOF **2** was evacuated at 150 °C for 12 h and further characterized by elemental analysis and TGA. A single crystal of **2′** suitable for XRD was obtained by slow thermal heating at a rate of 6 K min^{-1}, and data were collected at various temperature intervals (25−100 °C). It was observed that at 40 °C we could achieve an evacuated framework of **2** with reasonably good data [R_1 = 5.7%, wR_2 = 15.12%, GOF = 1.071]; below that temperature water stays in the lattice as solvent, and above it the framework remains intact but high thermal vibration in the atom sites results in high refinement parameters. Elemental analysis: calcd C (37.44%), H (4.28%), N (7.94%); found C (37.36%), H (4.21%), N (7.72%).

X-ray Crystallography. All single-crystal data were collected on a Bruker SMART APEX three-circle diffractometer equipped with a CCD area detector (Bruker Systems Inc.)[12a] and operated at 1500 W power (50 kV, 30 mA) to generate Mo Kα radiation (λ = 0.71073 Å). The incident X-ray beam was focused and monochromated using Bruker Excalibur Gobel mirror optics. Crystals of the Zn-MOFs reported in the paper were mounted on nylon CryoLoops (Hampton Research) with Paratone-N (Hampton Research). Data were integrated using Bruker SAINT software.[12b] Data were subsequently corrected for absorption by the program SADABS.[12c] Space group determinations and tests for merohedral twinning were carried out using XPREP. In all cases, the highest possible space group was chosen. All structures were solved by direct methods and refined using the SHELXTL 97[12d] software suite. Atoms were located from iterative examination of difference F-maps following least-squares refinements of the earlier models. Hydrogen atoms were placed in calculated positions and included as riding atoms with isotropic displacement parameters 1.2−1.5 × U_{eq} of the attached C atoms. Hydrogen atoms attached to the lattice water molecules in **1**−**4** could not be located or fixed. Data were collected at 196(2) K for MOFs **1**−**4**, 353(2) K for MOF **1**-evac (**1′**), and 313 (2) K for MOF **2**-evac (**2′**) reported in this paper. All structures were examined using the Addsym subroutine of PLATON[12e] to ensure that no additional symmetry could be applied to the models. All ellipsoids in ORTEP diagrams are displayed at the 50% probability level unless noted otherwise (Figure S15). The Supporting Information contains a detailed data collection strategy and crystallographic data (Tables S7 and S8) for the MOFs reported in this paper. Crystallographic data (excluding structure factors) for the structures reported in this paper have also been deposited with the CCDC as deposition Nos. CCDC 831054−831059 [available free of charge, on application to the CCDC, 12 Union Rd., Cambridge CB2 lEZ, U.K.; fax +44 (1223) 336 033; E-mail deposit@ccdc.cam.ac.uk].

RESULTS AND DISCUSSION

Synthesis and Characterization. Chirality, helicity, and porosity play important roles in chemistry and biology,[13] and it is a challenge to combine all these properties in a single domain. Construction of a helical MOF is fascinating, as helical assemblies such as protein bundles and DNA are prevalent in biological systems and play key roles in molecular recognition, replication, and catalysis.[14] Several approaches have been developed for constructing chiral MOFs with potential applications in the fields of chiral synthesis, optical devices, sensory functions, modeling of biological compounds, etc.[15] Multitopic linkers derived from natural amino acids,[16] because of their biological functional properties and highly selective substrate-binding abilities, are an attractive choice as chiral building blocks for the preparation of the aforementioned materials. Although Rosseinsky et al. reported diverse three-dimensional MOFs[16e−g] using pure amino acids and 4,4′-bipyridine-based ancillary ligands, chiral MOFs from amino acid-derived links that possess 3-D architecture as well as porosity are rare. Amino acid derivatives (links that have been synthesized from amino acids) are good choices over pure natural amino acids, as most of the latter prefer to chelate metal centers utilizing the amino and carboxylate groups to form mostly zero-/one-dimensional complexes. Recently, Wu et al. synthesized a serine derivative ligand which shows promising catalytic activity, but the resulting MOF adopts a 2D chain rather creating a 3D architecture.[16h] From the above facts, it is evident that amino acid derivatives (naturally available and pure enantiomer) are good choices as chiral links for designing 3D homochiral MOFs with various promising applications.

MOFs **1**−**4** reported in this paper were synthesized by mixing $Zn(CH_3COO)_2\cdot 2H_2O$ and 3-methyl-2-(pyridin-4-ylmethylamino)butanoic acid (a valine-derived link) (Figure 1a) under hydrothermal conditions in water medium. Phase-pure rod-shaped crystals were grown in a capped vial at 90 °C within 5−6 h. **1**−**4** are structural isomers with different anions (Cl^- or Br^-) coordinated to the metal atoms or enantiomers with respect to ligand backbone (*d* or *l*). MOF **1** crystallizes in the $P6_1$ space group, comprising one Zn(II), one ***l*-L$_{Cl}$** ligand, and two lattice water molecules in the asymmetric unit. The Zn(II) center adopts a distorted square pyramidal geometry (τ =0.88), chelated by monodentate carboxylate [(Zn1−O2 2.170(3) Å)] and one amino functionality [(Zn1−N1 2.092(4) Å)] of the first ***l*-L$_{Cl}$** link. One pyridyl functionality and one carboxyl oxygen atom of the second ***l*-L$_{Cl}$** ligand coordinate in the equatorial positions, and one free chlorine atom occupies the axial site (Figure 1b). Noticeably, the amine group is induced by the neighboring chiral carbon center into a homochiral unit to coordinate the zinc atom. As a result, the zinc atom acquires a third homochiral center associated with two homochiral centers. All adjacent zinc nodes are bridged by pyridyl groups to form a 6_1 helical chain with a pitch of 12 Å along the crystallographic *c*-axis (Figure 1c). The two coordinated carboxylate oxygens stay opposite to each other along the *c*-axis, through which additional molecules link to form the wall of the helical chain.

Among the pyridyl rings along the helical chain, one set of pridyl rings run in a clockwise direction while the others (linking two molecular chains) run anti-clockwise to extend the lattice along the *ab*-plane. This results in a 3D supramolecular network containing a close-packed 1D open channel along the *c*-axis filled with water molecules (Figure 2a). Pyridyl rings and isopropyl groups constitute the wall of the helical channel, providing a hydrophobic environment. This molecular arrangement result in a rare zeolitic *unh*-topology which has not been perceived so far in any synthetic means, even though it is theoretically proposed in ZIFs.[17] The *unh*-topology has a vertex symbol $5.5.5.5_2.12.12$ (Figure 2b). We analyzed the complexity of the nets in terms of their natural tiling, where the set of edges and vertices of the tiles is the same as that of the net.[18] MOFs **1**−**4** have a transitivity value of 1221, which means that the tiling has one kind of vertices, two kinds of edges, two kinds of faces, and one kind of tiles. MOFs **1**−**4** comprise a uninodal net having an isohedral kind of tile. The tile has two five-sided and two twelve-sided faces, with face symbol $5^2.12^2$ (Figure 2b). Lattice water molecules weakly H-bonded to the M−Cl atom (O···Cl−M, 3.175(1) Å) run along the helical channel (Figure 2c). The second water molecule resides within H-bonding distance of the first water molecule ($D_{O\cdots O}$ = 3.234(3)Å) to make a continuous water channel along the *c*-axis. This H-bonding distance is well within

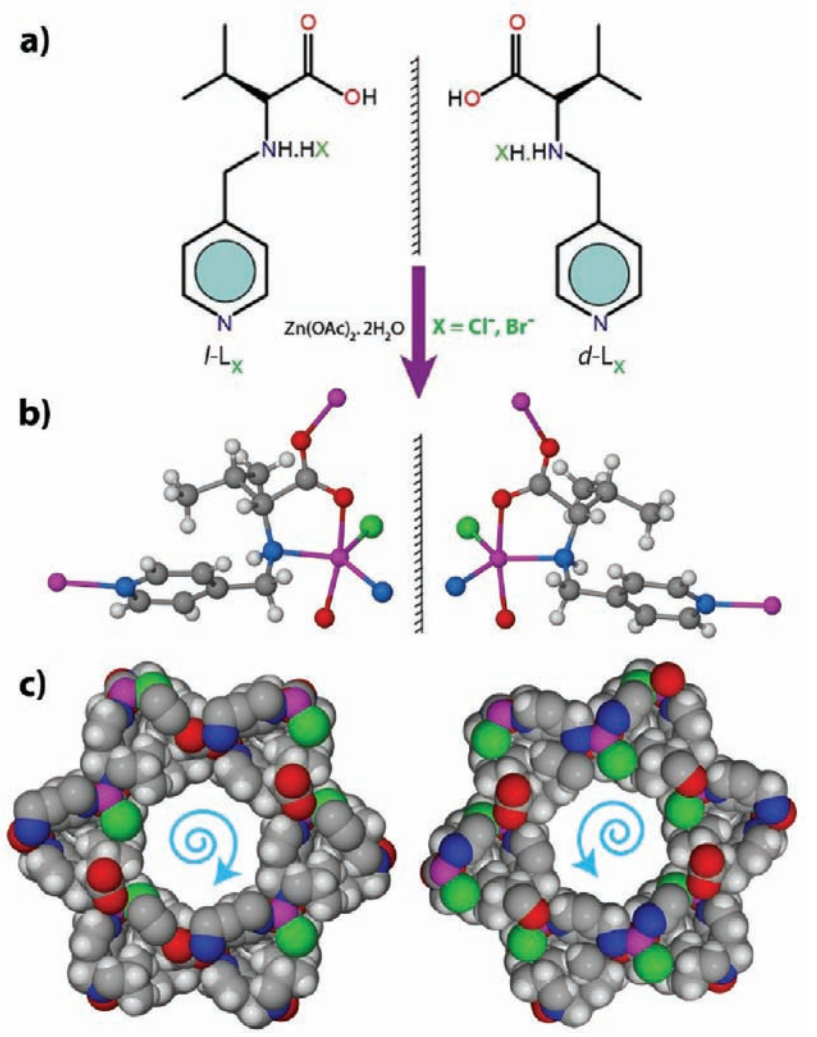

Figure 1. (a) Schematic representation of the links with mirror isomers (*l*-$\mathbf{L_X}$) and (*d*-$\mathbf{L_X}$) in the form of different salts, where X = Cl^-, Br^- are shown in green. (b) Ball-and-stick model of an asymmetric unit of MOFs with mirror isomers, showing a five-coordinated zinc center (pink ball). (c) Space-filling model of two enantiomers of MOF **1** and **3**. Opposite helicity is shown as a blue curved arrow. Color code: gray, Cl green, Cl; red, O; blue, N; pink, Zn; white, H.

the range of $D_{O\cdots O}$ of O−H···O hydrogen-bonding reported in the literature. As a result, a secondary helical water chain surrounded by the molecular helix is formed. Weak (O−H···Cl−M) H-bonding may allow the water protons to become more acidic. It was found that the helical orientation of water molecules is the structural basis by which K^+ ion and proton transport occurs inside a KcsA K^+ channel and in protein aquaporin-1, respectively.[19] 1D water chains also play vital roles for stabilizing the native conformation of biopolymers, but such helical water chains are less reported in synthetic homochiral crystal hosts,[20] espsecially in MOFs, because in most cases high-boiling solvents like DMF, DMA, DMSO, and DEF are used for MOF synthesis instead of water.

Single-crystal XRD analysis revealed that MOFs **2**, **3**, and **4** are isomorphous to MOF **1**, where **1**/**2** and **3**/**4** are isomers with respect to substituted halogen atoms, like **1** [L_2M-Cl] and **2** [L_2M-Br], but **1**/**3** and **2**/**4** are enantiomers. In **2**, each Zn^{II} cation has a similar coordination environment, except that the axial position is occupied by a Br atom. The trigonality factor τ is almost same (τ = 0.89) as that of **1**. Lattice water molecules are weakly H-bonded and placed almost in equivalent position with respect to the Br atom, showing a helical arrangement similar to that of **1**. For comparison, we prepared the enantiomer *d*-$\mathbf{L_{Cl}}$ analogue of **1**. The O···Br−M and O···O hydrogen-bonding distances in **2** are 3.175(1) and 3.34(7) Å, respectively. We obtained two enantiomorphic frameworks, $[Zn(d\text{-}\mathbf{L_{Cl}})(Cl)]\text{-}(H_2O)]_2$ (**3**) and $[Zn(d\text{-}\mathbf{L_{Br}})(Br)](H_2O)]_2$ (**4**), based on self-assembly between *d*-$\mathbf{L_{Cl}}$ and *d*-$\mathbf{L_{Br}}$ with $Zn(CH_3COO)_2\cdot 2H_2O$ under similar hydrothermal conditions. CD measurements on bulk crystals of **1** and **3** show opposite Cotton effects at ∼238 and 265 nm (Figure S22), indicating that **1**/**3** and **2**/**4** are enantiomers. The coordination environment of **3** and **4** is similar to that of **1** and **2**, except the resulting crystal structure adopts opposite handedness. **3** and **4** also contain two water molecules as lattice solvent, having weak H-bonding of 3.158 (O···Cl−M) and 3.175 Å (O···Br−M), respectively. Overall, it has been confirmed that all four isomers possess similar lattice arrangement (*unh*-topology) and the helical water chain persists irrespective of the different halogen substitution or change in chirality of the ligand backbone.

The phase purity of the bulk materials was confirmed by PXRD experiments, which are in good agreement with the

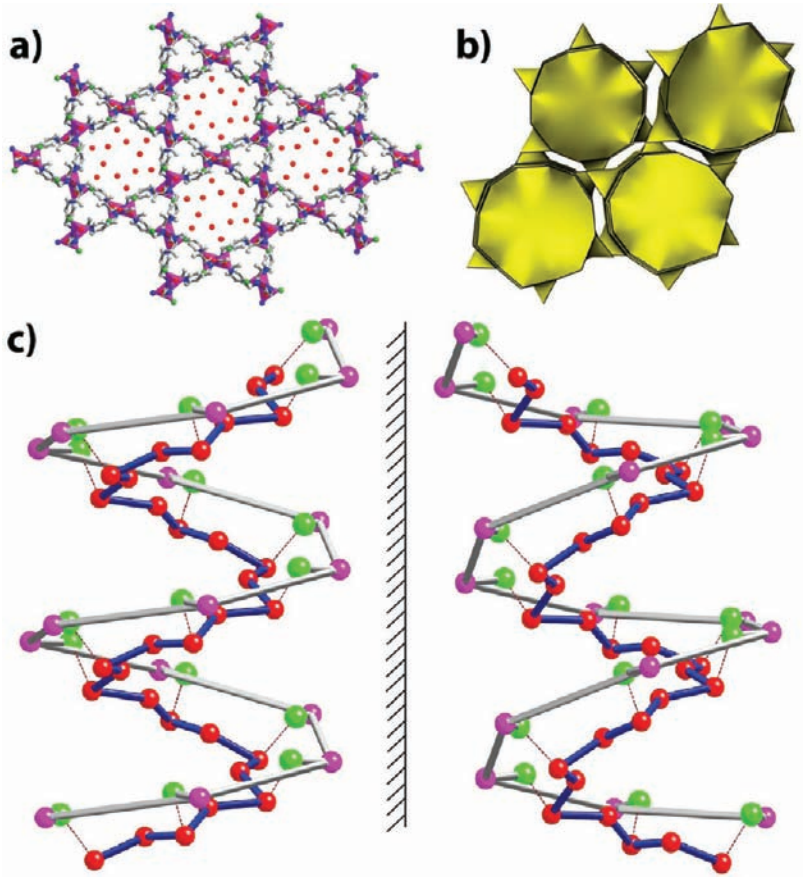

Figure 2. (a) Polyhedral representation of the MOF **1** lattice viewed down the *c*-axis. Pink polyhedra represent zinc centers, and lattice water molecules are shown as red balls. (b) Tiling figure of MOF **1**, showing zeolitic *unh*-topology along the *c*-axis. The tiling shows one kind of vertices, two kinds of edges, two kinds of faces, and one kind of tiles. (c) Mirror isomers of helical water chains surrounded by a molecular helix (outer helix). The molecular helix (outer helix) is shown as pink balls connected via gray bonds, and the helical water chain (inner helix) is shown as red balls connected via blue rods.

simulated PXRD patterns (Figures S2−S5). TGA performed on as-synthesized **1**−**4** revealed that these compounds have thermal stability up to ∼270 °C (Figure S17). The TGA trace for as synthesized **1**, **2**, **3** and **4** showed gradual weight-loss steps of ∼7% ($2H_2O$ in **1** and **3**, calcd 10.5%) and ∼6% ($2H_2O$ in **2** and **4**, calcd 9.3%) over a temperature range of 40−100 °C, corresponding to escape of guest water molecules from the pores (Figure S17). We note that the water molecules of **1** and **2** were released without damaging the frameworks, as evidenced by the coincidence of the PXRD patterns of **1** and **2** samples heated to and held at 150 °C in a N_2 atmosphere with the PXRD patterns simulated from single-crystal structures. The above fact is also verified by in situ VT-PXRD of MOF **1** (Figures 3a and S18) and MOF **2** (Figure S19). All major peaks of experimental and simulated PXRDs are well matched, indicating the sample's phase purity (Figure 3a). A combined heating and cooling in situ VT-PXRD experiment reveals that the framework is stable, remains crystalline over a wide temperature range (heating from 25 to 200 °C and then cooling from 200 to 25 °C), and remains stable after solvent removal (solvent escape ∼100 °C, confirmed by TGA). Escape of water molecules from the crystals was also monitored by hot-stage microscopy at different temperature intervals (25−270 °C). Pictures taken on a hot-stage microscope reveal that the trapped water molecules escape the lattice between 60 and 120 °C as heating goes on and cracking appears on the crystal surface, but crystallinity remains intact up to 250 °C (Figure S23). This observation indicates that it is possible to monitor the arrangement of water molecules with respect to temperature, and we can achieve a solvent-free framework after successful removal of solvent at higher temperatures.

It is noteworthy that the water molecules adopt similar arrangements in all MOFs **1**−**4** reported in this paper, except the handedness. The guest-free frameworks of MOFs **1**−**4** reported in this paper show high affinity for water, irrespective of different structural variation. It is worth mentioning that only a handful of Zn-based MOFs reported in literature can withstand moisture.[21]Upon exposure to moisture, Zn-based MOFs undergo phase transformation, which leads to decrease in gas sorption. Few well-known MOFs, like MOF-5[22a] and MOF 177,[22b] show this kind of behavior. Recently, water-stable, methyl-modified MOF-5 was successfully synthesized by incorporation of a methyl group in the parent ligand of MOF-5.[22c] To provide further evidence of water affinity apart from crystallographic information, MOF **1** was extensively studied by various experiments. MOF **1** shows a reversible transformation in the presence of water vapor. After evacuation at 150 °C for 2 days, the dehydrated polycrystalline sample of **1** (confirmed by PXRD, IR, and TGA) was exposed in a closed chamber saturated with water vapor. The single-crystalline nature of MOF **1** comes back within 6−12 h (Figure 4a), which is confirmed by IR, TGA, and crystallography. FT-IR spectra of the evacuated MOF **1** sample collected at time intervals of 1 h showed a gradual increase in the

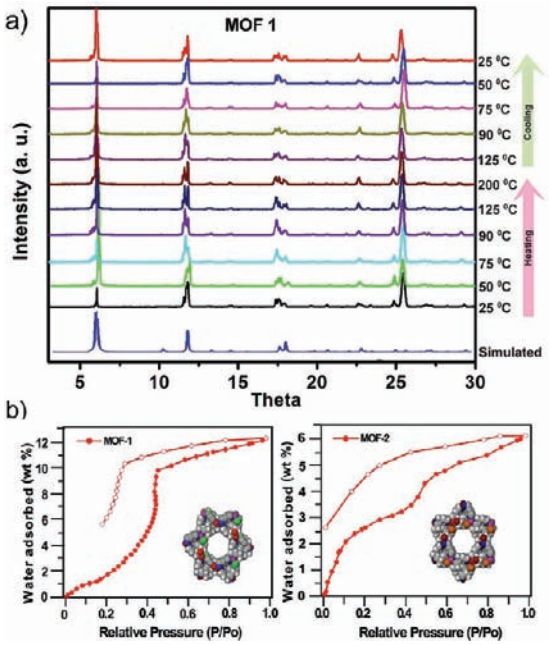

Figure 3. (a) In situ VT-PXRD of MOF **1** upon both heating (25−200 °C) and cooling (200−25 °C). This VT-PXRD experiment shows that the framework is stable and remains crystalline over a wide range of temperatures and after solvent removal. (b) Water adsorption isotherm of MOF **1** and MOF **2** showing 12 and 6 wt % of adsorption, respectively, at relative pressure $P/P_o = 0.9$.

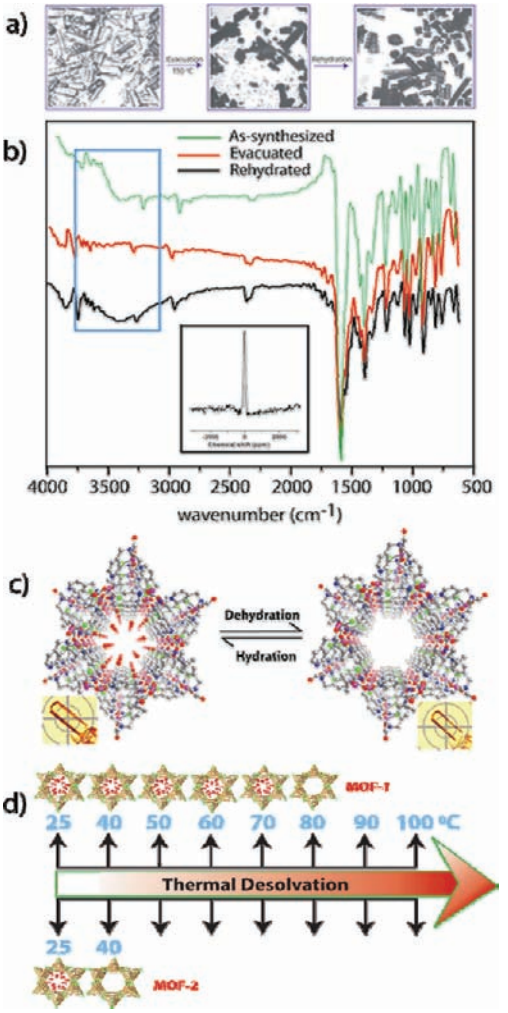

Figure 4. (a) Photographs of MOF **1** before and after evacuation at 150 °C, followed by rehydration showing reappearance of single crystallinity. (b) Appearance and disappearance of water peaks in IR spectra of as-synthesized, evacuated, and rehydrated MOF **1** confirms the reversible transformation. The SSNMR spectrum of MOF **1**-D_2O (D_2O-exchanged sample of MOF **1**) is shown in the inset. (c) Reversible crystal transformation of MOF **1** confirmed by in situ single-crystal XRD showing the MOF framework with/without solvent (water) as a ball-and-stick model along the *c*-axis. Crystallinity of MOF **1** remains intact and suitable for data collection over the temperature, as shown by crystal pictures taken during data collection. (d) Thermal desolvation and in situ VT single-crystal experiment of evacuated MOFs **1** and **2** achieved at 80 and 40 °C, respectively, confirms that MOF **2** has lower water holding capacity than MOF **1**.

intensity of the water peaks after exposure of **1** to moisture (Figure 4b), which further confirms the high affinity of **1** for water. The water affinity of **1** and **2** was also examined by water adsorption isotherms. Surprisingly, we found that MOF **1** shows 12 wt % water vapor uptake (150 cm^3/g at STP), whereas MOF **2** shows 6 wt % (75 cm^3/g at STP), about half at a relative pressure (P/P_o) of 0.9 (Figure 3b). It is quite clear that MOF **2** has less water affinity compared to MOF **1**, though the framework arrangements in **1** and **2** are similar. The CO_2 adsorption isotherm indicates much less uptake (25 cm^3/g for **1**, 20 cm^3/g for **2**) than predicted on the basis of X-ray crystallography and indicates a low degree of interaction points inside the pore (Figure S27).

Inspired by the above results, we thought to establish the above fact by in situ variable-temperature SCXRD. VT-SCXRD analyses of MOFs **1** and **2** were performed at different temperature intervals of 25, 40, 50, 60, 70, 80, 90, 100, and 115 °C. Before data collection, the crystallinity of MOFs was checked by taking snapshots and unit cell determination at each particular temperature to confirm that the sample's crystallinity remains intact, suitable for single-crystal data collection (Figures S20 and S21). From TGA experiments, it was found that the MOFs lose lattice water molecules in the temperature range of 40−80 °C. Taking a clue from the above observations, we anticipated not only that we could possibly achieve an evacuated framework via a SC-SC transformation but also that we can monitor the dynamics of H_2O inside the framework molecule over that temperature range. After carefully solving the above collected data sets, we found that 80 °C is the ideal temperature at which we could achieve a stable and solvent-free framework of **1** with reasonably good data [$R_1 = 6.4\%$, $wR_2 = 14.7\%$, GOF = 1.005]; below that temperature, water stays in the lattice as solvent and the framework remains intact, but high thermal vibration observed in some of the atom sites results in high refinement parameters (Figure 4d). A similar experiment performed on MOF **2** (−Br analogue of MOF **1**) reveals that we can achieve an evacuated framework at a much lower temperature of 40 °C [$R_1 = 5.7\%$, $wR_2 = 15.12\%$, GOF = 1.071]. So far, the amount of water uptake of MOF **1** with respect to MOF **2** and the achievement of an evacuated framework of MOF **2** at only 40 °C clearly indicate that MOF **2** has a lower water affinity than MOF **1**. It has been mentioned already that the structural arrangements of MOFs **1**−**4** are all similar, except for the handedness and halogen atoms in the framework [M−X, X = −Cl, −Br)]. It is well established that metal halides

dx.doi.org/10.1021/ja2078637 |*J. Am. Chem. Soc.* 2011, 133, 17950–17958

(M−X) are strong hydrogen bond acceptors, compared to organic halides (principally C−Cl and C−Br groups). The normalized distance function, R_{HX}, for D−H···X−M hydrogen bonds [$R_{HX} = d(H\cdots X)/(r_H + r_X)$ = 0.799 and 0.820 for O−H···X−M, X = Cl^-, Br^-)] shows the acceptor capabilities of halogens.[23,24] It is anticipated that, due to the increase in polarity of the D− H bond, for a given halide ion, O−H donors can contribute stronger interaction than N−H donors. Similarly, halide ion acceptors for a given donor are compared, and the interactions follow an order H···F > H···Cl > H···Br > H···I. In the present scenario for MOFs **1** and **2**, it is expected that O−H···X−M interaction is stronger in **1** (X = Cl^-) than **2** (X = Br^-).

The X-ray crystal structures of **1**−**4** established that these materials are amenable to proton-conduction owing to the continuous (O···O) helical 1D water chain ($D_{O\cdots O}$ = 3.234(3)Å) in a confined hydrophobic and acidic environment ($D_{O\cdots Cl-M}$ = 3.164 Å, $D_{O\cdots Br-M}$ = 3.175 Å). The proton conductivities of two halogen isomers, **1** and **3**, were measured by a quasi-two-probe method, with a Solartron 1287 electrochemical interface with frequency response analyzer. The conductivities were determined from the semicircles in the Nyquist plots (Figures 5 and S29). The proton conductivities of **1** and **3** were 4.45×10^{-5} and 4.42×10^{-5} S cm^{-1}, respectively, at 304 K and 98% relative humidity (RH). This value was highly humidity-dependent and dropped to 1.49×10^{-5} and 1.22×10^{-5} S cm^{-1} at 75% and 60% RH, respectively, at 304 K (Figure S29). Surprisingly, **2** and **4** show almost zero proton conductivity. Before coming to any conclusion, we tested the reproducibility by measuring the aforementioned proton conduction 4−5 times on different batches of samples. Each experiment revealed similar results.

The above anomalous behavior is attributed to a few reasons: (1) the water holding capacity of MOF **2** is less than that of MOF **1**, confirmed by water adsorption; (2) at room temperature (∼35 °C), MOF **1** has a continuous water chain, while MOF **2** has a discrete water assembly, confirmed by VT-SCXRD experiments; (3) the interior cavities with halogen atoms with different electronegativities are hydrogen bonded to water molecules. The present results also supported the lower water adsorption property shown by MOF **2** (6 wt %) compared to MOF **1** (12 wt %), as discussed previously. To prove the role of water molecules, we synthesized **1**-D_2O [$Zn(\mathit{l}\text{-}L_{cl})(Cl)(D_2O)$], taking D_2O as solvent of synthesis. **1**-D_2O was studied further by IR and ^2H SSNMR (Figures S8 and S24), which confirmed the D_2O incorporation in **1**-D_2O and its structural similarity to MOF **1**. Impedance studies on the deuterated sample in a H_2 atmosphere humidified (98%) with D_2O gave a conductivity value of 1.33×10^{-5} S cm^{-1}. The lower value is expected due to the heavier isotopic substitution. Proton conductivity measurements performed at different temperatures show a gradual increase in proton conductivity from 3.13×10^{-5} to 4.45×10^{-5} S cm^{-1} as the temperature is increased from 299 to 304 K, respectively (Figure 5b). At higher temperatures, above 40 °C, the proton conductivity of **1** decreases due to partial dehydration, as indicated by a TGA plot, and the ^2H SSNMR data had indicated mobile protons/deuterons even at 25 °C. A similar property was also observed for a previously reported MOF by Shimizu et al.[6b] The activation energies (E_a) for the proton transfer derived from the bulk conductivity of **1** and **3** were 0.34 and 0.36 eV, respectively, as determined from least-squares fits of the slopes. MOF **1** show a higher E_a value than Nafion (0.22 eV),[25b] but comparable with those of $Zr(HPO_4)_2$ (0.33)[25c] and $HUO_2PO_4 \cdot 4H_2O$ (0.32 eV).[25d] This low E_a observed in **1** indicates that the

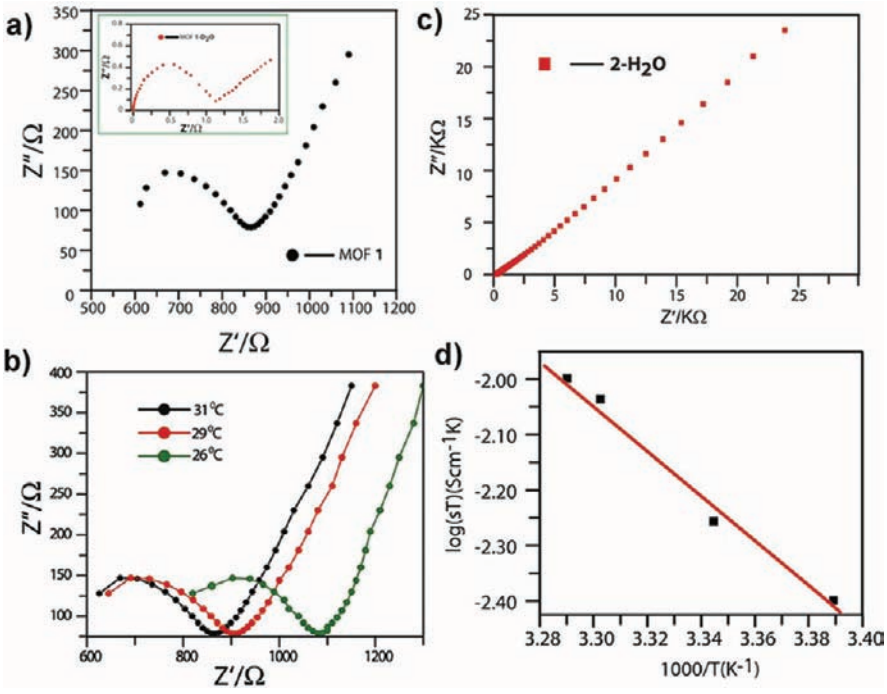

Figure 5. (a) Proton conductivity data comparison of MOF **1** and **1**-D_2O (inset) at 98% relative humidity (RH) showing decreasing proton conductivity value after D_2O substitution. (b) Temperature-dependent proton conductivity values of MOF **1** at different temperatures. (c) Proton conductivity of MOF **2** at 98% RH, showing zero proton conduction as compared to MOF **1** under similar conditions. (d) Arrhenius plots of proton conductivity of MOF **1**.

dx.doi.org/10.1021/ja2078637 |J. Am. Chem. Soc. 2011, 133, 17950–17958

ordered helical water chain (observed crystallographically) functions to transport protons via a Grotthuss hopping mechanism, as opposed to the higher E_a value observed for a vehicular transfer mechanism. The proton conductivity value of MOF **1** is higher than those of MIL-53-based MOFs ($\sim 10^{-6}$–10^{-9} S cm^{-1} reported by Kitagawa et al.[8c] at 25 °C, 95% RH) and comparable to that of a zinc-phosphonate MOF (1.33×10^{-5} S cm^{-1} reported by Shimizu et al.[6b] at 25 °C, 98% RH) but lower than those of a ferrous oxalate dihydrate (1.3×10^{-3} S cm^{-1} at 25 °C, 98% RH)[6c] and cucurbit[6]uril (1.1×10^{-3} S cm^{-1} at 25 °C, 98% RH)[27] under similar conditions (Table S9).

CONCLUSION

We have synthesized four new homochiral Zn-MOFs, **1**–**4**, using amino acid-derived links. These MOFs adopt 3D periodic architecture with 1D helical continuous water chains, irrespective of the type of halogen atom substitution or enantiomeric difference. All four MOFs **1**–**4** show an unprecedented zeolitic *unh*-topology which has not been perceived so far by any synthetic means. Two lattice water molecules along with another form a secondary helical water chain inside the molecular helix. In MOFs **1** and **2**, water escapes at ∼40–100 °C, but they show reversible crystallization by readily reabsorbing moisture, which is also confirmed by VT-PXRD experiments. The hydrophobic environment of the 1D channel along with weak H-bonding with halogen atoms provides a facile pathway for proton conduction in humid conditions. In MOFs **1** and **3**, this is the first example in which proton conductivity has been observed in chiral MOFs having helical water chains confined in a hydrophobic and acidic environment controlled by metal-bound halogen atoms. Substitution of different halogen atom results in anomalous proton conductivity behavior of MOFs **1** and **3** with respect to MOFs **2** and **4**. High water uptake capacity, high water holding capacity, and high electronegativity of chlorine with respect to bromine may explain the higher proton conductivity value of MOF **1** than MOF **2**. Stronger O–H···Cl–M interactions result in increasing acidity of the water protons and subsequently become the major driving force of proton conduction in MOF **1** relative to **2**. The role of the water chain in proton conduction has been further confirmed by D_2O-exchange experiments. Ion conduction in MOFs has been reported in only a handful of cases. These results provide a good roadmap toward tuning and precisely controlling the proton conductivity and consequently will enable us to develop useful domains both for solid electrolytes and from the biological perspective.

ASSOCIATED CONTENT

Supporting Information. Experimental details and characterization data, including X-ray crystallographic data. This material is available free of charge via the Internet at http://pubs.acs.org.

AUTHOR INFORMATION

Corresponding Author
sc.sahoo@ncl.res.in; r.banerjee@ncl.res.in

ACKNOWLEDGMENT

S.C.S. acknowledges CSIR, New Delhi, India, for a CSIR Nehru science postdoctoral research fellowship. T.K. acknowledges CSIR, New Delhi, India, for a JRF. R.B. acknowledges CSIR's XIth Five Year Plan Project (NWP0022-H and NWP0021-A) for funding and also Dr. S. Pal, S. Sivaram, B. D. Kulkarni, and K. Vijaymohanan for their encouragement. Financial assistance from the DST (SR/S1/IC-22/2009) is acknowledged.

REFERENCES

(1) (a) Chae, H. K.; Siberio-Perez, D. Y.; Kim, J.; Go, Y.; Eddaoudi, M.; Matzger, A. J.; O'Keeffe, M.; Yaghi, O. M. *Nature* **2004**, *427*, 523. (b) Zhao, X.; Xiao, B.; Fletcher, J. A.; Thomas, K. M.; Bradshaw, D.; Rosseinsky, M. J. *Science* **2004**, *306*, 1012. (c) Ferey, G.; Mellot-Draznieks, C.; Serre, C.; Millange, F.; Dutour, J.; Surble, S.; Margiolaki, I. *Science* **2005**, *309*, 2040. (d) Chandler, B. D.; Enright, G. D.; Udachin, K. A.; Pawsey, S.; Ripmeester, J. A.; Cramb, D. T.; Shimizu, G. K. H. *Nat. Mater.* **2008**, *7*, 229.

(2) (a) Lee, J. Y.; Farha, O. K.; Roberts, J.; Scheidt, K. A.; Nguyen, S. T.; Hupp, J. T. *Chem. Soc. Rev.* **2009**, *38*, 1450. (b) Seo, J. S.; Whang, D.; Lee, H.; Jun, S. I.; Oh, J.; Jeon, Y. J.; Kim, K. *Nature* **2000**, *404*, 982. (c) Zou, R.-Q.; Sakurai, H.; Xu, Q. *Angew. Chem., Int. Ed.* **2006**, *45*, 2542.

(3) (a) Kurmoo, M. *Chem. Soc. Rev.* **2009**, *38*, 1353. (b) Tamaki, H.; Zhong, Z. J.; Matsumoto, N.; Kida, S.; Koikawa, M.; Achiwa, N.; Hashimoto, Y.; Okawa, H. *J. Am. Chem. Soc.* **1992**, *114*, 6974. (c) Ohba, M.; Okawa, H. *Coord. Chem. Rev.* **2000**, *198*, 313. (d) Shiga, T.; Okawa, H.; Kitagawa, S.; Ohba, M. *J. Am. Chem. Soc.* **2006**, *128*, 16426.

(4) (a) Kitagawa, H.; Onodera, N.; Sonoyama, T.; Yamamoto, M.; Fukuwa, T.; Mitani, T.; Seto, M.; Maeda, Y. *J. Am. Chem. Soc.* **1999**, *121*, 10068. (b) Fuma, Y.; Ebihara, M.; Kutsumizu, S.; Kawamura, T. *J. Am. Chem. Soc.* **2004**, *126*, 12238. (c) Otsubo, K.; Kobayashi, A.; Kitagawa, H.; Hedo, M.; Uwatoko, Y.; Sagayama, H.; Wakabayashi, Y.; Sawa, H. *J. Am. Chem. Soc.* **2006**, *128*, 8140. (d) Nagao, Y.; Fujishima, M.; Ikeda, R.; Kanda, S.; Kitagawa, H. *Synth. Met.* **2003**, *133*, 431. (e) Nagao, Y.; Kubo, T.; Nakasuji, K.; Ikeda, R.; Kojima, T.; Kitagawa, H. *Synth. Met.* **2005**, *154*, 89. (f) Okawa, H.; Shigematsu, A.; Sadakiyo, M.; Miyagawa, T.; Yoneda, K.; Ohba, M.; Kitagawa, H. *J. Am. Chem. Soc.* **2009**, *131*, 13516. (g) Yamada, T.; Morikawa, S.; Kitagawa, H. *Bull. Chem. Soc. Jpn.* **2010**, *83*, 42. (h) de Combarieu, G.; Morcrette, M.; Millange, F.; Guillou, N.; Cabana, J.; Grey, C. P.; Margiolaki, I.; Fe rey, G.; Tarascon, J. M. *Chem. Mater.* **2009**, *21*, 1602. (i) Ferey, G.; Millange, F.; Morcrette, M.; Serre, C.; Doublet, M. L.; Greneche, J. M.; Tarascon, J. M. *Angew. Chem., Int. Ed.* **2007**, *46*, 3259. (j) de Combarieu, G.; Hamelet, S.; Millange, F.; Morcrette, M.; Tarascon, J. M.; Férey, G.; Walton, R. I. *Electrochem. Commun.* **2009**, *11*, 1881. (k) Ohkoshi, S.; Nakagawa, K.; Tomono, K.; Imoto, K.; Tsunobuchi, Y.; Tokoro, H. *J. Am. Chem. Soc.* **2010**, *132*, 6620. (l) Hurd, J. A.; Vaidhyanathan, R.; Thangadurai, V.; Ratcliffe, C. I.; Moudrakovski, I. M.; Shimizu, G. K. H. *Nat. Chem.* **2009**, *1*, 705. (m) Duan, C. Y.; Wei, M. L.; Guo, D.; He, C.; Meng, Q. J. *J. Am. Chem. Soc.* **2010**, *132*, 3321.

(5) (a) Wood, B. C.; Marzari, N. *Phys. Rev. B* **2007**, *76*, 134301. (b) Kreuer, K. D.; Paddison, S. J.; Spohr, E.; Schuster, M. *Chem. Rev.* **2004**, *104*, 4637. (c) Hickner, M. A.; Ghassemi, H.; Kim, Y. S.; Einsla, B. R.; McGrath, J. E. *Chem. Rev.* **2004**, *104*, 4587. (d) Akutu-Sato, A.; Akutsu, H.; Turner, S. S.; Day, P.; Probert, M. R.; Howard, J. A. K.; Akutagawa, T.; Takeda, S.; Nakamura, T.; Mori, T. *Angew. Chem., Int. Ed.* **2005**, *44*, 292. (e) Steele, B. C.; Heinzel, A. *Nature* **2001**, *414*, 345. (f) Saiz, L.; M. Klein, L. *Acc. Chem. Res.* **2002**, *35*, 482. (g) Sapronova, A.; Bystrov, V. S.; Green, M. E. *Front. Biosci.* **2003**, *8*, 1356. (h) *Proton Conductors: Solids, Membranes and Gels—Materials and Devices. Series: Chemistry of Solid State Materials*, 2nd ed.; Colomban, P., Ed.; Cambridge University Press: Cambridge, UK, 1992. (i) Zhou, Z.; Li, S.; Zhang, Y.; Liu, M. *J. Am. Chem. Soc.* **2005**, *127*, 10824.

(6) (a) Shimizu, G. K. H.; Vaidhyanathan, R.; Taylor, J. M. *Chem. Soc. Rev.* **2009**, *38*, 1430. (b) Taylor, J. M.; Mah, R. K.; Moudrakovski, I. L.; Ratcliffe, C. I.; Vaidhyanathan, R.; Shimizu, G. K. H. *J. Am. Chem. Soc.* **2010**, *132*, 14055. (c) Kreuer, K. D. *Annu. Rev. Mater. Res.* **2003**, *33*, 333. (d) Schuster, M. F. H.; Meyer, W. H. *Annu. Rev. Mater. Res.* **2003**, *33*, 233. (e) Schuster, M. F. H.; Meyer, W. H.; Schuster, M.; Kreuer, K. D. *Chem. Mater.* **2004**, *16*, 329. (f) Maruitz, K. A.;

Moore, R. B. *Chem. Rev.* **2004**, *104*, 4535. (g) Casciola, M.; Alberti, G.; Sganappa, M.; Narducci, R. *J. Power Sources* **2006**, *162*, 141. (h) Hasegawa, S.; Horike, S.; Matsuda, R.; Furukawa, S.; Mochizuki, K.; Kinoshita, Y.; Kitagawa, S. *J. Am. Chem. Soc.* **2007**, *129*, 2607. (i) Matsuda, R.; Kitaura, R.; Kitagawa, S.; Kubota, Y.; Belosludov, R. V.; Kobayashi, T. C.; Sakamoto, H.; Chiba, T.; Takata, M.; Kawazoe, Y. *Nature* **2005**, *436*, 238.

(7) (a) Bureekaew, S.; Horike, S.; Higuchi, M.; Mizuno, M.; Kawamura, T.; Tanaka, D.; Yanai, N.; Kitagawa, S. *Nat. Mater.* **2009**, *8*, 831. (b) Li, S.; Zhou, Z.; Zhang, Y.; Liu, M. *Chem. Mater.* **2005**, *17*, 5884. (c) Nagao, Y.; et al. *Synth. Met.* **2005**, *154*, 892. (d) Nagao, Y.; Fujishima, M.; Ikeda, R.; Kanda, S.; Kitagawa, H. *Synth. Met.* **2003**, *133*, 43.

(8) (a) Sadakiyo, M.; Yamada, T.; Kitagawa, H. *J. Am. Chem. Soc.* **2009**, *131*, 9906. (b) Yamada, T.; Sadakiyo, M.; Kitagawa, H. *J. Am. Chem. Soc.* **2009**, *131*, 3144. (c) Shigematsu, A.; Yamada, T.; Kitagawa, H. *J. Am. Chem. Soc.* **2011**, *133*, 2034. (d) Morikawa, S.; Yamada, T.; Kitagawa, H. *Chem. Lett.* **2009**, *38*, 654.

(9) (a) Pomes, R.; Roux, B. *Biophys. J.* **1998**, *75*, 33. (b) Pomes, R.; Roux, B. *Biophys. J.* **2002**, *82*, 2304. (c) Cowin, J. P.; Tsekouras, A. A.; Iedema, M. J.; Wu, K.; Ellison, G. B. *Nature* **1999**, *398*, 405.

(10) (a) Lee, J. Y.; Roberts, J. M.; Farha, O. K.; Sarjeant, A. A.; Scheidt, K. A.; Hupp, J. T. *Inorg. Chem.* **2009**, *48*, 9971. (b) Li, J. R.; Tao, Y.; Yu, Q.; Bu, X. H.; Sakamoto, H.; Kitagawa, S. *Chem.—Eur. J.* **2008**, *14*, 2771. (c) Roswell, J. L. C.; Yaghi, O. M. *J. Am. Chem. Soc.* **2006**, *128*, 1304. (d) Furukawa, H.; Ko, N.; Go, Y. B.; Aratani, N.; Choi, S. B.; Choi, E.; Yazaydin, A. O.; Snurr, R. Q.; O'Keeffe, M.; Kim, J.; Yaghi, O. M. *Science* **2010**, *239*, 424. (e) Deng, H.; Doonan, C. J.; Furukawa, H.; Ferreira, R. B.; Towne, J.; Knobler, C. B.; Wang, B.; Yaghi, O. M. *Science* **2010**, *327*, 846.

(11) (a) Koh, L. L.; Ranford, J. O.; Robinson, W. T.; Svensson, J. O.; Tan, A. L. C.; Wu, D. *Inorg. Chem.* **1996**, *35*, 6466.

(12) (a) *APEX2*, Version 5.053; Bruker AXS Inc.: Madison,WI, 2005. (b) *SAINT-Plus*, Version 7.03; Bruker AXS Inc.: Madison, WI, 2004. (c) Sheldrick, G. M. *SADABS*, Version 2.03, and *TWINABS*, Version 1.02; University of Göttingen: Göttingen, Germany, 2002. (d) Sheldrick, G. M. *SHELXS '97 and SHELXL '97*; University of Göttingen: Göttingen, Germany, 1997. (e) Spek, A. L. *PLATON*, A Multipurpose Crystallographic Tool; Utrecht University: Utrecht, The Netherlands, 2005.

(13) (a) Valente, C.; Choi, E.; Belowich, M. E.; Doonan, C. J.; Li, Q.; Gasa, T. B.; Botros, Y. Y.; Yaghi, O. M.; Stoddart, J. F. *Chem. Commun.* **2010**, *46*, 4911. (b) Morris, R. E.; Bu, X. *Nature Chem.* **2010**, *2*, 353.

(14) (a) Berry, A.; Watson, J. D. *DNA: the secret of life*; Alfred A. Knopf: New York, 2003.

(15) (a) Ma, L.; Wu, C.; Wanderley, M. M.; Lin, W. *Angew. Chem., Int. Ed.* **2010**, *49*, 8244. (b) Ma, L.; Falkowski, J. M.; Abney, C.; Lin, W. *Nature Chem.* **2010**, *2*, 838. (c) Wu, C.-D.; Hu, A.; Zhang, L.; Lin, W. *J. Am. Chem. Soc.* **2005**, *127*, 8940. (d) Ong, T. T.; Kavuru, P.; Nguyen, T.; Cantwell, R.; Wojtas, L.; Zaworotko, M. *J. Am. Chem. Soc.* **2011**, *133*, 9224.

(16) (a) Ganguly, R.; Sreenivasulu, B.; Vittal, J. J. *Coord. Chem. Rev.* **2008**, *252*, 1027. (b) Sreenivasulu, B.; Vittal, J. J. *Angew. Chem., Int. Ed.* **2004**, *43*, 5769. (c) Alam, M.; Nethaji, M.; Ray, M. *Angew. Chem., Int. Ed.* **2003**, *42*, 1940. (d) Sahoo, C. S.; Ray, M. *Chem.—Eur. J.* **2010**, *16*, 5004. (e) Vaidhyanathan, R.; Bradshaw, D.; Rebilly, J.-N.; Barrio, J. P.; Gould, J. A.; Berry, N. G.; Rosseinsky, M. J. *Angew. Chem., Int. Ed.* **2006**, *45*, 6495. (f) Rebilly, J.; Gardner, P. W.; Darling, G. R.; Bacsa, J.; Rosseinsky, M. J. *Inorg. Chem.* **2008**, *47*, 9390. (g) Bradshaw, D.; Claridge, J. B.; Cussen, E. J.; Prior, T. J.; Rosseinsky, M. J. *Acc. Chem. Res.* **2005**, *38*, 273. (h) Wang, M.; Xie, M.; Wu, C.; Wang, Y. *Chem. Commun.* **2009**, 2396.

(17) (a) Baburin, I. A.; Leoni, S.; Seifert, G. *J. Phys. Chem. B* **2008**, *112*, 9437.

(18) (a) O'Keefee, M.; Peskov, M. A.; Ramsden, S. J.; Yaghi, O. M. *Acc. Chem. Res.* **2008**, *41*, 1782. (b) Tranchemontagne, D. J.; Mendoza-Cortes, J. L.; O'Keeffe, M.; Yaghi, O. M. *Chem. Soc. Rev.* **2009**, *38*, 1257.

(19) (a) Mitsuoka, K.; Murata, K.; Walz, T.; Hirai, T.; Agre, P.; Heymann, J. B.; Engel, A.; Fujiyoshi, Y. *J. Struct. Biol.* **1999**, *128*, 34. (b) Doyle, D. A.; Cabral, J. M.; Pfuetzner, R. A.; Kuo, A.; Gulbis, J. M.; Cohen, S. L.; Chait, B. T.; MacKinnon, R. *Science* **1998**, *280*, 69.

(20) (a) Ludwig, R. *Angew. Chem.* **2001**, *113*, 1856. *Angew. Chem., Int. Ed.* **2001**, *40*, 1808. (b) Konozo, D.; Yasui, M.; King, L. S.; Agre, P. *J. Clin. Invest.* **2002**, *109*, 1395. (c) Roux, B.; MacKinnon, R. *Science* **1999**, *285*, 100. (d) Buck, U.; Huisken, F. *J. Am. Chem. Soc.* **2000**, *100*, 3863.

(21) (a) Park, K. S.; Ni, Z.; Cote, A. P.; Choi, J. Y.; Huang, R.; Uribe-Romo, F. J.; Chae, H. K.; O'Keeffe, M.; Yaghi, O. M. *Proc. Natl. Acad. Sci. U.S.A.* **2006**, *103*, 10186. (b) Banerjee, R.; Phan, A.; Wang, B.; Knobler, C.; Furukawa, H.; O'Keeffe, M.; Yaghi, O. M. *Science* **2008**, *319*, 939. (c) Banerjee, R.; Furukawa, H.; Britt, D.; Knobler, C.; O'Keeffe, M.; Yaghi, O. M. *J. Am. Chem. Soc.* **2009**, *131*, 3875.

(22) (a) Li, H.; Eddaoudi, M.; O'Keeffe, M.; Yaghi, O. M. *Nature* **1999**, *402*, 276. (b) Chae, H. K.; Siberio-Perez, D. Y.; Kim, J.; Go, Y.-B.; Eddaoudi, M.; Matzger, A. J.; O'Keeffe, M.; Yaghi, O. M. *Nature* **2004**, *427*, 523. (c) Yang, J.; Grzech, A.; Mulder, F. M.; Dingemans, T. J. *Chem. Commun.* **2011**, *47*, 5244.

(23) Brammer, L.; Bruton, E. A.; Sherwood, P. *Cryst. Growth Des.* **2001**, *1*, 277.

(24) (a) Bentrup, U.; Feist, M.; Kemnitz, E. *Prog. Solid State Chem.* **1999**, *27*, 75. (b) Kuhlman, R. *Coord. Chem. Rev.* **1997**, *167*, 205.

(25) (a) Alberti, G.; Casciola, M. *Solid State Ionics* **2001**, *145*, 3. (b) Hainovsky, N. G.; Pavlukhin, Y. T.; Hairetdinov, E. F. *Solid State Ionics* **1986**, *20*, 249. (c) Bernard, L.; Fitch, A.; Wright, A. F.; Fender, B. E. F.; Howe, A. T. *Solid State Ionics* **1981**, *5*, 459. (d) Howe, A. T.; Shilton, M. G. *J. Solid State Chem.* **1979**, *28*, 345.

(26) Shigematsu, A.; Yamada, T.; Kitagawa, H. *J. Am. Chem. Soc.* **2011**, *133*, 2034.

(27) Yoon, M.; Suh, K.; Kim, H.; Kim, Y.; Selvapalam, N.; Kim, K. *Angew. Chem., Int. Ed.* **2011**, *50*, 7870.